A copper diimine-based honeycomb-like porous network as an efficient reduction catalyst

Journal:	*Applied Organometallic Chemistry*
Manuscript ID	AOC-20-0524.R1
Wiley - Manuscript type:	Full Paper
Date Submitted by the Author:	20-Sep-2020
Complete List of Authors:	Ahmad, Abrar ; Quaid-i-Azam University, Chemistry Shah, Syed Niaz Ali; Tsinghua University, Chemistry Arshad, Mehwish; Quaid-i-Azam University, chemistry Bélanger-Gariepy, Francine ; Universite de Montreal, Département de Chimie, A634 Tiekink, Edward; Sunway University, Center for Crystalline materials, School of Science and Technology Ur-Rehman, Zia; Quaid-i-Azam University, Chemistry
Keywords:	Porous network, Zeolite-like channels, Copper complex, Catalyst
Note: The following files were submitted by the author for peer review, but cannot be converted to PDF. You must view these files (e.g. movies) online.	
Scheme_cdx.cdx 1580602.cif	

Copper diimine-based honeycomb-like porous network

A copper diimine-based honeycomb-like porous network as an efficient reduction catalyst

Abrar Ahmad[a], Syed Niaz Ali Shah[a], Mehwish Arshad[a], Francine Bélanger-Gariepy[b], Edward R.T. Tiekink[c], Zia ur Rehman[a]*

[a] Department of Chemistry Quaid-i-Azam University Islamabad-45320, Pakistan.

[b] Département de Chimie, Université de Montréal, Montreal, Canada.

[c] Research Centre for Crystalline Materials, School of Science and Technology, Sunway University, 47500 Bandar Sunway, Selangor Darul Ehsan, Malaysia

***Corresponding author**

Email: zrehman@qau.edu.pk / hafizqau@yahoo.com

Tel: 0092-(051)90642245

Fax: 0092-(051)90642241

Copper diimine-based honeycomb-like porous network

Abstract

Nitrophenols are amongst the widely used industrial chemicals worldwide; however, their hazardous effects on environment are a major concern nowadays. Therefore, the conversion of environmentally detrimental *p*-nitrophenol (PNP) to industrially valuable *p*-aminophenol (PAP), a prototype reaction, is an important organic transformation reaction. However, the traditional conversion of PNP to PAP is an expensive and environment unfriendly process. Here, we report a honeycomb-like porous network with zeolite-like channels formed by the self-organization of copper, 1,10-phenanthroline, 4,4′-bipyridine and water. This porous network effectively catalyzed the transformation of hazardous PNP to pharmaceutically valued PAP. In the presence of complex, PNP to PAP conversion occurred in a few minutes, which is otherwise a very sluggish process. To assess the kinetics, the catalytic conversion of PNP to PAP was studied at five different temperatures. The linearity of $\ln C_t/C_o$ vs temperature plot indicated pseudo-first-order kinetics. The copper complex with zeolite like channels may find applications as a reduction catalyst both on laboratory and industrial scales, and in green chemistry for the remediation of pollutants.

Keywords: Porous network; Zeolite-like channels; Copper complex; Catalyst

Copper diimine-based honeycomb-like porous network

1. Introduction

Nitrophenols are amongst the most widely used industrial chemicals worldwide due to their applications in explosives, pesticides, dyes, and rubber materials [1]. However, owing to their carcinogenic and hazardous nature, the US Environmental Protection Agency (EPA) has enlisted them amongst the top organic pollutants [2]. Once internalized in the bloodstream, nitrophenols can cause variety of problems including methemoglobinemia, decrease ATP production, lungs damage, effect the nervous system, dermatitis, hormonal disorders, renal failure, skin damages, and eyes irritations [3].

To remove this stable, water-soluble, and environmentally hazardous [4] material several strategies have been employed, including adsorption [5], microbial degradation [6], photocatalytic degradation [7], the electro-Fenton method [8], electrocoagulation [9] and electrochemical treatment [10]. The conversion of environmentally detrimental *p*-nitrophenol (PNP) to industrially valuable *p*-aminophenol (PAP) is a very important organic transformation reaction. The latter being used in various antipyretic and analgesic drugs such as paracetamol, corrosion inhibitor, lubricant, and dyeing agent [11]. However, the traditional conversion of PNP to PAP is carried out in organic solvent under high pressure making this an expensive and environmentally non-friendly process [12].

To ensure the foregoing conversion in an inexpensive and environment-friendly manner, a smart strategy is usually adopted, that is, *via* a catalytic reduction in aqueous media. In this context, various metal-based nanocatalysts including those of Au [12-13], Ag [14], Pd [15], Cu [16], Zn, and Ni [17] have been used. To further enhance the stability and catalytic efficacy, these materials can be supported on polymers, oxides, resins, TiO_2, SiO_2, and carbon. Furthermore, some of these metals (e.g., Au, Pd, and Pt) are too expensive for

practical applications on a large scale. Literature studies reveal that photocatalytic reduction of PNP are mostly carried out by heterogeneous catalysis using various metal based nanostructures [18-20]. However, no homogenous catalyst has been reported so far to reduce PNP to PAP.

Sparked by the challenge that coordination chemistry could be exploited to mimic naturally occurring three-dimensional materials [21], crystal engineers have responded with a literal plethora of metal-organic framework (MOF) sustained by a combination of covalent/dative bonding interactions between practically all available metals and a huge diversity in ligands [22]. The opportunities for tuning/fine tuning synthetic outcomes by combining metal centers, e.g., choice of metal, oxidation state and coordination geometry preference, with ligands, e.g., charged or neutral, variable donor atoms and denticity, are enormous. Conversely, this variety of options coupled with the observation that reaction outcomes are sometimes dependent on the solvent, temperature, concentration of reagents, etc. [23], means there is practically an unlimited number of MOFs that can be generated. All this, of course, ignores two-dimensional coordination polymers, the focus of the present report, let alone one-dimensional chains. Links between lower-dimensional architectures can be anyone or a combination of noncovalent interactions [24], with hydrogen bonding obviously being prominent [25] but halogen bonding [26] and interactions involving "metalloligands" [27] also being important.

Recently copper based catalysts, owing to their impressive advantages over other transition metal catalysts, have received a significant attention. Their lower cost, readily availability, insensitivity to air, easy handling and generation of less waste make them versatile catalysts in various organic reaction like synthesis of enzymes [28], oxidative polymerization of aniline [29],

rearrangement reactions of aldoxime [30], reductions of nitroarenes [20] etc. Furthermore, copper is the second abundant transition metal inside human body, and can be easily metabolized by the body metabolic system [31]. Its antimicrobial nature and biocompatible features make it a suitable catalyst for biological applications [32].

Among the myriad of practical applications of MOF materials, owing to their zeolite-like pores, subsequent high surface area, and stability, relates to their high catalytic potential [21, 22], which indeed has inspired a large number of recent reviews on the utility of both transition metal- and lanthanide-based coordination polymers for catalytic applications [33]. Literature survey shows that the incorporation of PNP and BH_4^- into the pores of a porous structure have also been observed in case of certain porous zeolites [34] and MOFs supported photocatalyst [35].

During our on-going studies in copper chemistry [36], a zero-dimensional copper diimine complex, whereby the dimer is connected into a three-dimensional architecture *via* conventional hydrogen bonding interactions to generate a honeycomb-like porous network, has been synthesized, characterized, and investigated as a catalyst for PNP reduction to PAN.

2. Materials and methods

Analytical grade chemicals were purchased from Merck (copper(II) chloride dihydrate) Sigma-Aldrich (1,10-phenanthroline, 4,4′-bipyridine, sodium borohydride, silver nitrate, and ethanol) and Fluka (*p*-nitrophenol) companies.

2.1. Synthesis of the copper diimine complex

An ethanolic solution (25 mL) of 1,10-phenanthroline (0.58 g, 2.9 mmol) was added dropwise to a $CuCl_2.2H_2O$ (0.50 g, 2.9 mmol) solution (25 mL) in the same solvent, and the

mixture was stirred for 30 min at room temperature. The light blue precipitates thus obtained were filtered off and dried in the open air. The precipitates (0.714 g, 2.27 mmol) were re-dissolved in distilled water in a two-necked flask and treated with $AgNO_3$ (0.77 g, 4.51 mmol) in the dark and stirred for 24 h. To remove AgCl, the solution was filtered and to this, an ethanolic solution of 4,4′-bipyridine (0.35 g, 2.27 mmol) was added dropwise followed by reflux at 110 °C till the turbidity cleared (Scheme 1). Blue crystals were obtained from the slow evaporation of the final filtered solution. Yield 78% (0.54 g); m.p. 270-272 °C; FT-IR (cm^{-1}): 3441 ν (O-H), 3040 ν (C-H)aromatic; 1659 ν (C=N); 1612 ν (C=C)aromatic; 1522 ν (ring vibration; 1494) ν $(N-O)_{asym}$; 1305 ν $(N-O)_{sym}$.

2.2. Characterization

Gallenkamp (UK) electrothermal melting point apparatus, UV-Visible spectrophotometer (Model TCC-240A, CAT. No. 204-05557) Shimadzu 1800 double beam (Japan) and Perkin Elmer Spectrum 1000 (USA) instruments were used for recording melting point, time-dependent UV-Vis and FT-IR spectra, respectively.

2.3. Single crystal study

Intensity data for a blue block (0.08 x 0.20 x 30 mm) were measured at 100 K on a Bruker Venture Metal jet diffractometer using Ga Kα radiation (λ = 1.34139 Å) so that $2\theta_{max}$ = 54.9°. A total of 69840 absorptions corrected [37] data were collected of which 11307 were unique (R_{int} = 0.051) and of these, 9908 satisfied the $I \geq 2\sigma(I)$ criterion. The structure was solved by SHELXT [38] and refined on F^2 with SHELXL-2014/7 [39] integrated within Olex [40]. Non-hydrogen atoms were refined anisotropically and non-acidic H atoms were included in the model in their calculated positions. The water-H atoms were located and

refined without restraint. At this stage of the refinement, the presence of heavily disordered solvent molecules, i.e., ethanol and water were indicated. These were modeled employing the SQUEEZE routine [41] with full details given in the deposited CIF. The final refinement (701 parameters) had a weighting scheme of the form w = 1/[s2(Fo2) + 0.052P2 + 13.335P] where $P = (F_o^2 + 2F_c^2)/3$) on F^2 and converged with $R = 0.065$ and $wR2 = 0.171$. The molecular structure diagram was generated with ORTEP for Windows [42] at the 35% probability level and the packing diagrams were drawn with DIAMOND [43].

Crystal data for $C_{54}H_{44}Cu_2N_{12}O_8$ (1); exclusive of unresolved solvent) M = 1116.09, monoclinic space group $P2_1/c$, a = 7.3006(2), b = 43.8747(10), c = 18.6593(4) Å, β = 94.4600(10)°, V = 5958.7(2) Å^3, Z = 4, D_x = 1.244 g cm^{-3}, μ = 4.166 mm^{-1}. CCDC deposition number: 1580602.

3. RESULTS AND DISCUSSIONS

3.1. Crystal and molecular structures

The molecular structure along with crystallographic numbering scheme for the binuclear copper complex is shown in Figure 1. While the structure is devoid of crystallographic symmetry, it has pseudo two-fold symmetry with the axis bisecting the central C–C bond of the bridging 4,4'-bipyridyl (bipy) ligand and lying in the plane of defined by Cu1, Cu3, N1, and N31 atoms. The coordination geometry for the Cu1 atom is defined by N atoms of the chelating 1,10-phenanthroline (phen) ligand, an N atom of one end of the bridging bipy ligand, an N atom of a terminally bound bipy ligand, an aqua-O atom and one O atom of the nitrate anion. The immediate environment of the Cu1 atom is defined by the N_4O_2 donor set and is best described as 5+1 as the Cu–O63 bond length is significantly longer

than the other bonds as seen from the data collated in Table 1; an analogous coordination geometry is seen for the Cu3 atom. Nevertheless, the coordination geometry is based on an octahedron. There is a small number of literature precedents for the aforementioned structure. Thus, the $Cu_2(phen)_2(bipy)_3$ fragment has been observed in the structure of the copper(II) complex [(L-valinato-N,O)(bipy)(H_2O) Cu(bipy)Cu(L-valinato-N,O)(bipy)(OH_2)](NO_3)$_2$.2H_2O [44] but where the terminal bipy ligands have an anti-disposition as opposed to *syn* in 1; the Cu atoms have square pyramidal geometries with aqua ligands in the apical positions. An anti-disposition is also found in the structure of [(phen)(bipyH)(H_2O)Cu(bipy)Cu(phen)(bipyH)(OH_2)][$Mo_{12}O_{40}P$]$_2$.2H_2O [45], i.e., with protonated terminally bound bipy ligands, where the bulky counter ions cannot approach the copper centers resulting in square pyramidal geometries again with the aqua ligands in the apical positions. Of particular interest in the structure of 1 is the mode of supramolecular aggregation occurring in the crystal.

As anticipated, conventional hydrogen bonding plays a significant role in the molecular packing of 1, (Table S1). Thus, aqua-O–H···O(nitrate) hydrogen bonds, involving both pairs of independent aqua molecules and nitrate anions, leads to the formation of supramolecular chains along the *a*-axis. As viewed from Figure 2a, the chain is linear and as both terminal bipy molecules are oriented to the same side, the topology is of a U-tube. The remaining aqua-H atoms form hydrogen bonds to the non-coordinating pyridyl-N atoms derived from two symmetry-related U-tubes, of opposite orientation, to generate layers in the *ac*-plane and, crucially, approximately square channels parallel to *a*-axis direction (Figure 2b). The channels have disparate edge lengths and the maximum dimensions of the face, based on the Cu···Cu separations, are 8.8 x 11.0 x 12.0 x 13.1 Å. The

layers stack along the *b*-axis with the primary connections between them being of the type phen-C–H···O(nitrate) (Table S1). In this way, additional channels are formed which is more symmetrical with each edge, again based on Cu···Cu separations, being 10.7 Å (Figure 2c).

3.2. Catalytic activity

The catalytic ability of 1 was evaluated for the PNP's reduction into PAP using $NaBH_4$, a prototype reaction. The reduction was followed readily by UV-visible spectroscopy as both reactant (PNP) and product (PAP) absorb in the UV-visible region at different λ_{max} values [46]. Without a catalyst, the only obvious change noted was deepening of the yellow appearance of PNP upon the addition of $NaBH_4$ accompanied by a redshift (317 nm to 400 nm), signifying the formation of PNP ions (Figure S1). The absence of a peak pertinent to PAP, even after keeping the solution for several days, indicated that the reaction required a catalyst to proceed [47]. However, in the presence of 1, PNP to PAP conversion occurred after a few minutes as signified by the diminishing of the peak of PNP (400 nm) and the emergence of a new peak for PAP at 290 nm [48] (Figure 3a-e). In the induction period, the time required for the diffusion of reagents and catalyst, $\ln C_t/C_o$ value remains unchanged. Excess $NaBH_4$ was used, and the linearity of $\ln C_t/C_o$ vs temperature relationship indicated pseudo first-order kinetics [49]. Afterward, the catalytic conversion of PNP to PAP was studied at five different temperatures (Figure 3a-e). The induction time decreases as does the reaction time, i.e. from 22 min (25 °C) to 5 min (45 °C). Furthermore, a threefold increase in the apparent rate constant was witnessed as the temperature rose from 25 to 45 °C (Figure 4). This correlated with an increase in the average kinetic energy of molecules at elevated temperature which in turn increases the diffusion rate of the reactants. Hence, an

increase in collision frequency and a fast diffusion rate triggered the conversion of reactants into products [50]. The Arrhenius equation i.e., $lnk = ln\ A - E_a/RT$, was used to calculate E_a by plotting lnk vs $1/T$ gives a slope E_a/RT that corresponds E_a value of 40.65 kJmol^{-1} [51]. The kinetic parameters such as activation entropy ($\Delta S^{\#}$) and enthalpy ($\Delta H^{\#}$) were calculated using the Erying equation i.e., $lnk/T = ln(k_b/h) + \Delta S^{\#}/R - \Delta H^{\#}/R\ (1/T)$ [52], where T is the absolute temperature, k_b is the Boltzmann constant, h is the Planck constant, and R is the ideal gas constant. The plot of lnk_{app}/T vs $1/T$ gives a straight line with slope $-\Delta H^{\#}/R$ (Figure 5) and intercept ($ln(k_b/h) + \Delta S^{\#}/R$) from which $-\Delta H^{\#}$ (38.09 kJmol^{-1}) and $\Delta S\#$ (-197.51 Jmol^{-1} K^{-1}) can be calculated (Table 2). The positive $\Delta H^{\#}$ value reflects the endothermic nature of the reduction process.

4. CONCLUSIONS

Crystallography established **1** to contain well-defined channels which, when evacuated can accommodate guest species to facilitate the conversion of environmentally detrimental PNP to pharmaceutically useful PAP. It can be envisaged that the cationic form of the complex **1**, after ionization of NO_3^-, has a high affinity for PNP and BH_4^- anions which are encapsulated in the pores to undergo the redox reaction. PNP to PAP conversion, which otherwise not possible in the absence of a suitable catalyst, completed within a few minutes in the presence of **1**. This study demonstrated that **1** with zeolite like channels can find applications as a reduction catalyst both on laboratory and industrial scales, and catalyze reactions of environmental significance.

ASSOCIATED CONTENT

Supporting Information

Copper diimine-based honeycomb-like porous network

Supporting information contains details of the specified intermolecular interactions (Table S1) and UV-visible spectra of *p*-nitrophenol and *p*-nitrophenolate ion (Figure S1). The Supporting Information is available free of charge on the WileyPublications website.

AUTHOR INFORMATION

Corresponding Author

* Zia-ur-Rehman (zrehman@qau.edu.pk / hafizqau@yahoo.com), Tel: 92-(051)90642245

Fax: 92-(051)90642241

Note

There is no conflict of interest.

ACKNOWLEDGMENT

We acknowledge the financial support from the Higher education Commission of Pakistan.

Data Availability statement

The authors confirm that the data supporting the findings of this study are available within the article and its supplementary materials.

Copper diimine-based honeycomb-like porous network

References

[1] F.-h. Lin, R.-a. Doong, *Applied Catalysis A: General* **2014**, *486*, 32-41.

[2] J. Feng, L. Su, Y. Ma, C. Ren, Q. Guo, X. Chen, *Chemical engineering journal* **2013**, *221*, 16-24.

[3] P. K. Arora, A. Srivastava, V. P. Singh, *Journal of hazardous materials* **2014**, *266*, 42-59.

[4] Z. Dong, X. Le, C. Dong, W. Zhang, X. Li, J. Ma, *Applied Catalysis B: Environmental* **2015**, *162*, 372-380.

[5] E. Marais, T. Nyokong, *Journal of hazardous materials* **2008**, *152*, 293-301.

[6] O. A. O'Connor, L. Young, *Environmental toxicology and chemistry* **1989**, *8*, 853-862.

[7] M. S. Dieckmann, K. A. Gray, *Water Research* **1996**, *30*, 1169-1183.

[8] M. A. Oturan, J. Peiroten, P. Chartrin, A. J. Acher, *Environmental Science & Technology* **2000**, *34*, 3474-3479.

[9] N. Modirshahla, M. Behnajady, S. Mohammadi-Aghdam, *Journal of hazardous materials* **2008**, *154*, 778-786.

[10] P. Canizares, C. Saez, J. Lobato, M. Rodrigo, *Industrial & engineering chemistry research* **2004**, *43*, 1944-1951.

[11] S. Saha, A. Pal, S. Kundu, S. Basu, T. Pal, *Langmuir* **2009**, *26*, 2885-2893.

[12] Y.-C. Chang, D.-H. Chen, *Journal of hazardous materials* **2009**, *165*, 664-669.

[13] a) D. Huang, G. Yang, X. Feng, X. Lai, P. Zhao, *New Journal of Chemistry* **2015**, *39*, 4685-4694; b) P. Pachfule, S. Kandambeth, D. D. Díaz, R. Banerjee, *Chemical Communications* **2014**, *50*, 3169-3172; c) R. Fenger, E. Fertitta, H. Kirmse, A. Thünemann, K. Rademann, *Physical Chemistry Chemical Physics* **2012**, *14*, 9343-9349.

Copper diimine-based honeycomb-like porous network

[14] a) P. Zhang, C. Shao, Z. Zhang, M. Zhang, J. Mu, Z. Guo, Y. Liu, *Nanoscale* **2011**, *3*, 3357-3363; b) Z. Wang, S. Zhai, B. Zhai, Z. Xiao, F. Zhang, Q. An, *New Journal of Chemistry* **2014**, *38*, 3999-4006; c) S. Xiao, W. Xu, H. Ma, X. Fang, *RSC Advances* **2012**, *2*, 319-327.

[15] a) C. Deraedt, L. Salmon, D. Astruc, *Advanced Synthesis & Catalysis* **2014**, *356*, 2525-2538; b) Z. Wang, C. Xu, G. Gao, X. Li, *RSC Advances* **2014**, *4*, 13644-13651; c) X. Gu, W. Qi, X. Xu, Z. Sun, L. Zhang, W. Liu, X. Pan, D. Su, *Nanoscale* **2014**, *6*, 6609-6616.

[16] a) A. K. Patra, A. Dutta, A. Bhaumik, *Catalysis Communications* **2010**, *11*, 651-655; b) P. Deka, R. C. Deka, P. Bharali, *New Journal of Chemistry* **2014**, *38*, 1789-1793; c) P. Zhang, Y. Sui, G. Xiao, Y. Wang, C. Wang, B. Liu, G. Zou, B. Zou, *Journal of Materials Chemistry A* **2013**, *1*, 1632-1638.

[17] A. Goyal, S. Bansal, S. Singhal, *international journal of hydrogen energy* **2014**, *39*, 4895-4908.

[18] H. Zhang, S. Gao, N. Shang, C. Wang, Z. Wang, RSC advances, 4 (2014) 31328-31332.

[19] J. Li, L. Zhang, X. Liu, N. Shang, S. Gao, C. Feng, C. Wang, Z. Wang, New Journal of Chemistry, 42 (2018) 9684-9689.

[20] H. Zhang, Y. Zhao, W. Liu, S. Gao, N. Shang, C. Wang, Z. Wang, Catalysis Communications, 59 (2015) 161-165.

[21] B. Hoskins, R. Robson, *Journal of the American Chemical Society* **1990**, *112*, 1546-1554.

[22] P. Z. Moghadam, A. Li, S. B. Wiggin, A. Tao, A. G. Maloney, P. A. Wood, S. C. Ward, D. Fairen-Jimenez, *Chemistry of Materials* **2017**, *29*, 2618-2625.

[23] a) B. Moulton, M. J. Zaworotko, *Chemical Reviews* **2001**, *101*, 1629-1658; b) A. J. Howarth, Y. Liu, P. Li, Z. Li, T. C. Wang, J. T. Hupp, O. K. Farha, *Nature Reviews Materials* **2016**, *1*, 15018.

[24] a) K. T. Mahmudov, M. N. Kopylovich, M. F. C. G. da Silva, A. J. Pombeiro, *Coordination Chemistry Reviews* **2017**, *345*, 54-72; b) E. R. Tiekink, *Coordination Chemistry Reviews* **2017**, *345*, 209-228.

[25] a) J. Reedijk, *Chemical Society Reviews* **2013**, *42*, 1776-1783; b) N. Adarsh, P. Dastidar, *Chemical Society Reviews* **2012**, *41*, 3039-3060.

[26] a) K. Rissanen, *CrystEngComm* **2008**, *10*, 1107-1113; b) B. Li, S.-Q. Zang, L.-Y. Wang, T. C. Mak, *Coordination Chemistry Reviews* **2016**, *308*, 1-21.

[27] a) S. J. Garibay, J. R. Stork, S. M. Cohen, *Progress in Inorganic Chemistry, Volume 56* **2009**, 335-378; b) G. Kumar, R. Gupta, *Chemical Society Reviews* **2013**, *42*, 9403-9453.

[28] F. Chen, Y. Chen, H. Cao, Q. Xu, L. Yu, The Journal of Organic Chemistry, 83 (2018) 14158-14164.

[29] Y. Chen, Q. Zhang, X. Jing, J. Han, L. Yu, Materials Letters, 242 (2019) 170-173.

[30] F. Xin, Y. Rong, W. Fang, Z. Xu, X. Qing, Y. Lei, Chinese Journal of Organic Chemistry, 38 (2018) 2736-2740.

[31] D. Soriano del Amo, W. Wang, H. Jiang, C. Besanceney, A.C. Yan, M. Levy, Y. Liu, F.L. Marlow, P. Wu, Journal of the American Chemical Society, 132 (2010) 16893-16899.

[32] A.P. Ingle, N. Duran, M. Rai, Applied Microbiology and Biotechnology, 98 (2014) 1001-1009.

[33] a) A. Zanon, F. Verpoort, *Coordination Chemistry Reviews* **2017**, *353*, 201-222; b) K. Vellingiri, L. Philip, K.-H. Kim, *Coordination Chemistry Reviews* **2017**, *353*, 159-179; c) Z.

Hu, D. Zhao, *CrystEngComm* **2017**, *19*, 4066-4081; d) Q. Yang, Q. Xu, H.-L. Jiang, *Chemical Society Reviews* **2017**, *46*, 4774-4808; e) L. Zhu, X.-Q. Liu, H.-L. Jiang, L.-B. Sun, *Chemical Reviews* **2017**, *117*, 8129-8176; f) C. Pagis, M. Ferbinteanu, G. Rothenberg, S. Tanase, *ACS Catalysis* **2016**, *6*, 6063-6072.

[34] S. Oh, S. Lee, M. Oh, ACS Applied Materials & Interfaces, 12 (2020) 18625-18633.

[35] M.A. Ahsan, E. Deemer, O. Fernandez-Delgado, H. Wang, M.L. Curry, A.A. El-Gendy, J.C. Noveron, Catalysis Communications, 130 (2019) 105753.

[36] M. Iqbal, S. Ali, Z.-U. Rehman, N. Muhammad, M. Sohail, V. Pandarinathan, *Journal of Coordination Chemistry* **2014**, *67*, 1731-1745.

[37] V. SAINT, *Madison, WI, USA* **2014**.

[38] S. Version, *Acta Crystallogr., Sect. A: Found. Crystallogr* **2008**, A64.

[39] G. M. Sheldrick, *Acta Crystallographica Section C: Structural Chemistry* **2015**, *71*, 3-8.

[40] O. V. Dolomanov, A. J. Blake, N. R. Champness, M. Schröder, *Journal of applied crystallography* **2003**, *36*, 1283-1284.

[41] P. SQUEEZE, *Acta Crystallographica, Section C: Structural Chemistry* **2015**, *71*, 9-18.

[42] L. J. Farrugia, *Journal of applied crystallography* **2012**, *45*, 849-854.

[43] C. Impact, *Crystal Impact GbR, Bonn, Germany* **2006**.

[44] B.-Y. Lou, M.-C. Hong, *Acta Crystallographica Section E: Structure Reports Online* **2008**, *64*, m405-m405.

[45] D.-D. Yang, B. Mu, L. Lv, R.-D. Huang, *Journal of Coordination Chemistry* **2015**, *68*, 752-765.

[46] N. Sahiner, S. Butun, O. Ozay, B. Dibek, *Journal of colloid and interface science* **2012**, *373*, 122-128.

[47] M. Nasrollahzadeh, S. M. Sajadi, A. Rostami-Vartooni, M. Bagherzadeh, *Journal of colloid and interface science* **2015**, *448*, 106-113.

[48] K. Kuroda, T. Ishida, M. Haruta, *Journal of Molecular Catalysis A: Chemical* **2009**, *298*, 7-11.

[49] a) S. ur Rehman, M. Siddiq, H. Al-Lohedan, N. Sahiner, *Chemical engineering journal* **2015**, *265*, 201-209; b) X. Le, Z. Dong, W. Zhang, X. Li, J. Ma, *Journal of Molecular Catalysis A: Chemical* **2014**, *395*, 58-65.

[50] S. Wu, J. Dzubiella, J. Kaiser, M. Drechsler, X. Guo, M. Ballauff, Y. Lu, *Angewandte Chemie International Edition* **2012**, *51*, 2229-2233.

[51] M. Ajmal, Z. H. Farooqi, M. Siddiq, *Korean Journal of Chemical Engineering* **2013**, *30*, 2030-2036.

[52] a) N. Sahiner, N. Karakoyun, D. Alpaslan, N. Aktas, *International Journal of Polymeric Materials and Polymeric Biomaterials* **2013**, *62*, 590-595; b) S. Butun, N. Sahiner, *Polymer* **2011**, *52*, 4834-4840.

A copper diimine-based honeycomb-like porous network as an efficient reduction catalyst

Abrar Ahmad[a], Syed Niaz Ali Shah[a], Mehwish Arshad[a], Francine Bélanger-Gariepy[b], Edward R.T. Tiekink[c], Zia ur Rehman[a]*

[a] Department of Chemistry Quaid-i-Azam University Islamabad-45320, Pakistan.

[b] Département de Chimie, Université de Montréal, Montreal, Canada.

[c] Research Centre for Crystalline Materials, School of Science and Technology, Sunway University, 47500 Bandar Sunway, Selangor Darul Ehsan, Malaysia

***Corresponding author**

Email: zrehman@qau.edu.pk / hafizqau@yahoo.com

Tel: 0092-(051)90642245

Fax: 0092-(051)90642241

Copper diimine-based honeycomb-like porous network

Abstract

Nitrophenols are amongst the widely used industrial chemicals worldwide; however, their hazardous effects on environment are a major concern nowadays. Therefore, the conversion of environmentally detrimental *p*-nitrophenol (PNP) to industrially valuable *p*-aminophenol (PAP), a prototype reaction, is an important organic transformation reaction. However, the traditional conversion of PNP to PAP is an expensive and environment unfriendly process. Here, we report a honeycomb-like porous network with zeolite-like channels formed by the self-organization of copper, 1,10-phenanthroline, 4,4′-bipyridine and water. This porous network effectively catalyzed the transformation of hazardous PNP to pharmaceutically valued PAP. In the presence of complex, PNP to PAP conversion occurred in a few minutes, which is otherwise a very sluggish process. To assess the kinetics, the catalytic conversion of PNP to PAP was studied at five different temperatures. The linearity of $\ln C_t/C_o$ vs temperature plot indicated pseudo-first-order kinetics. The copper complex with zeolite like channels may find applications as a reduction catalyst both on laboratory and industrial scales, and in green chemistry for the remediation of pollutants.

Keywords: Porous network; Zeolite-like channels; Copper complex; Catalyst

Copper diimine-based honeycomb-like porous network

1. Introduction

Nitrophenols are amongst the most widely used industrial chemicals worldwide due to their applications in explosives, pesticides, dyes, and rubber materials [1]. However, owing to their carcinogenic and hazardous nature, the US Environmental Protection Agency (EPA) has enlisted them amongst the top organic pollutants [2]. Once internalized in the bloodstream, nitrophenols can cause variety of problems including methemoglobinemia, decrease ATP production, lungs damage, effect the nervous system, dermatitis, hormonal disorders, renal failure, skin damages, and eyes irritations [3].

To remove this stable, water-soluble, and environmentally hazardous [4] material several strategies have been employed, including adsorption [5], microbial degradation [6], photocatalytic degradation [7], the electro-Fenton method [8], electrocoagulation [9] and electrochemical treatment [10]. The conversion of environmentally detrimental *p*-nitrophenol (PNP) to industrially valuable *p*-aminophenol (PAP) is a very important organic transformation reaction. The latter being used in various antipyretic and analgesic drugs such as paracetamol, corrosion inhibitor, lubricant, and dyeing agent [11]. However, the traditional conversion of PNP to PAP is carried out in organic solvent under high pressure making this an expensive and environmentally non-friendly process [12].

To ensure the foregoing conversion in an inexpensive and environment-friendly manner, a smart strategy is usually adopted, that is, *via* a catalytic reduction in aqueous media. In this context, various metal-based nanocatalysts including those of Au [12-13], Ag [14], Pd [15], Cu [16], Zn, and Ni [17] have been used. To further enhance the stability and catalytic efficacy, these materials can be supported on polymers, oxides, resins, TiO_2, SiO_2, and carbon. Furthermore, some of these metals (e.g., Au, Pd, and Pt) are too expensive for practical applications on a large

scale. Literature studies reveal that photocatalytic reduction of PNP are mostly carried out by heterogeneous catalysis using various metal based nanostructures [18-20] . However, no homogenous catalyst has been reported so far to reduce PNP to PAP.

Sparked by the challenge that coordination chemistry could be exploited to mimic naturally occurring three-dimensional materials [21], crystal engineers have responded with a literal plethora of metal-organic framework (MOF) sustained by a combination of covalent/dative bonding interactions between practically all available metals and a huge diversity in ligands [22]. The opportunities for tuning/fine tuning synthetic outcomes by combining metal centers, e.g., choice of metal, oxidation state and coordination geometry preference, with ligands, e.g., charged or neutral, variable donor atoms and denticity, are enormous. Conversely, this variety of options coupled with the observation that reaction outcomes are sometimes dependent on the solvent, temperature, concentration of reagents, etc. [23], means there is practically an unlimited number of MOFs that can be generated. All this, of course, ignores two-dimensional coordination polymers, the focus of the present report, let alone one-dimensional chains. Links between lower-dimensional architectures can be anyone or a combination of noncovalent interactions [24], with hydrogen bonding obviously being prominent [25] but halogen bonding [26] and interactions involving "metalloligands" [27] also being important.

Recently copper based catalysts, owing to their impressive advantages over other transition metal catalysts, have received a significant attention. Their lower cost, readily availability, insensitivity to air, easy handling and generation of less waste make them versatile catalysts in various organic reaction like synthesis of enzymes [28], oxidative polymerization of aniline [29], rearrangement reactions of aldoxime [30] , reductions of nitroarenes [20] etc. Furthermore, copper is the second abundant transition metal inside human body, and can be easily metabolized

by the body metabolic system [31]. Its antimicrobial nature and biocompatible features make it a suitable catalyst for biological applications [32].

Among the myriad of practical applications of MOF materials, owing to their zeolite-like pores, subsequent high surface area, and stability, relates to their high catalytic potential [21, 22], which indeed has inspired a large number of recent reviews on the utility of both transition metal- and lanthanide-based coordination polymers for catalytic applications [33]. Literature survey shows that the incorporation of PNP and BH_4^- into the pores of a porous structure have also been observed in case of certain porous zeolites [34] and MOFs supported photocatalyst [35].

During our on-going studies in copper chemistry [36], a zero-dimensional copper diimine complex, whereby the dimer is connected into a three-dimensional architecture *via* conventional hydrogen bonding interactions to generate a honeycomb-like porous network, has been synthesized, characterized, and investigated as a catalyst for PNP reduction to PAN.

2. Materials and methods

Analytical grade chemicals were purchased from Merck (copper(II) chloride dihydrate) Sigma-Aldrich (1,10-phenanthroline, 4,4′-bipyridine, sodium borohydride, silver nitrate, and ethanol) and Fluka (*p*-nitrophenol) companies.

2.1. Synthesis of the copper diimine complex

An ethanolic solution (25 mL) of 1,10-phenanthroline (0.58 g, 2.9 mmol) was added dropwise to a $CuCl_2.2H_2O$ (0.50 g, 2.9 mmol) solution (25 mL) in the same solvent, and the mixture was stirred for 30 min at room temperature. The light blue precipitates thus obtained were filtered off and dried in the open air. The precipitates (0.714 g, 2.27 mmol) were re-dissolved in distilled water in a two-necked flask and treated with $AgNO_3$ (0.77 g, 4.51 mmol) in the dark and stirred

for 24 h. To remove AgCl, the solution was filtered and to this, an ethanolic solution of 4,4′-bipyridine (0.35 g, 2.27 mmol) was added dropwise followed by reflux at 110 °C till the turbidity cleared (Scheme 1). Blue crystals were obtained from the slow evaporation of the final filtered solution. Yield 78% (0.54 g); m.p. 270-272 °C; FT-IR (cm^{-1}): 3441 ν (O-H), 3040 ν (C-H)aromatic; 1659 ν (C=N); 1612 ν (C=C)aromatic; 1522 ν (ring vibration; 1494) ν $(N-O)_{asym}$; 1305 ν $(N-O)_{sym}$.

2.2. Characterization

Gallenkamp (UK) electrothermal melting point apparatus, UV-Visible spectrophotometer (Model TCC-240A, CAT. No. 204-05557) Shimadzu 1800 double beam (Japan) and Perkin Elmer Spectrum 1000 (USA) instruments were used for recording melting point, time-dependent UV-Vis and FT-IR spectra, respectively.

2.3. Single crystal study

Intensity data for a blue block (0.08 x 0.20 x 30 mm) were measured at 100 K on a Bruker Venture Metal jet diffractometer using Ga Kα radiation (λ = 1.34139 Å) so that $2\theta_{max}$ = 54.9°. A total of 69840 absorptions corrected [37] data were collected of which 11307 were unique (R_{int} = 0.051) and of these, 9908 satisfied the $I \geq 2\sigma(I)$ criterion. The structure was solved by SHELXT[38] and refined on F^2 with SHELXL-2014/7 [39] integrated within Olex [40]. Non-hydrogen atoms were refined anisotropically and non-acidic H atoms were included in the model in their calculated positions. The water-H atoms were located and refined without restraint. At this stage of the refinement, the presence of heavily disordered solvent molecules, i.e., ethanol and water, were indicated. These were modeled employing the SQUEEZE routine [41] with full details given in the deposited CIF. The final refinement (701 parameters) had a weighting

scheme of the form w = 1/[s2(Fo2) + 0.052P2 + 13.335P] where $P = (F_o^2 + 2F_c^2)/3)$ on F^2 and converged with $R = 0.065$ and $wR2 = 0.171$. The molecular structure diagram was generated with ORTEP for Windows [42] at the 35% probability level and the packing diagrams were drawn with DIAMOND [43].

Crystal data for $C_{54}H_{44}Cu_2N_{12}O_8$ (**1**); exclusive of unresolved solvent) $M = 1116.09$, monoclinic space group $P2_1/c$, $a = 7.3006(2)$, $b = 43.8747(10)$, $c = 18.6593(4)$ Å, $\beta = 94.4600(10)°$, $V = 5958.7(2)$ Å^3, $Z = 4$, $D_x = 1.244$ g cm^{-3}, $\mu = 4.166$ mm^{-1}. CCDC deposition number: 1580602.

3. RESULTS AND DISCUSSIONS

3.1. Crystal and molecular structures

The molecular structure along with crystallographic numbering scheme for the binuclear copper complex is shown in Figure 1. While the structure is devoid of crystallographic symmetry, it has pseudo two-fold symmetry with the axis bisecting the central C–C bond of the bridging 4,4'-bipyridyl (bipy) ligand and lying in the plane of defined by Cu1, Cu3, N1, and N31 atoms. The coordination geometry for the Cu1 atom is defined by N atoms of the chelating 1,10-phenanthroline (phen) ligand, an N atom of one end of the bridging bipy ligand, an N atom of a terminally bound bipy ligand, an aqua-O atom and one O atom of the nitrate anion. The immediate environment of the Cu1 atom is defined by the N_4O_2 donor set and is best described as 5+1 as the Cu–O63 bond length is significantly longer than the other bonds as seen from the data collated in Table 1; an analogous coordination geometry is seen for the Cu3 atom. Nevertheless, the coordination geometry is based on an octahedron. There is a small number of literature precedents for the aforementioned structure. Thus, the $Cu_2(phen)_2(bipy)_3$ fragment has been observed in the structure of the copper(II) complex [(L-valinato-N,O)(bipy)(H_2O)

Cu(bipy)Cu(L-valinato-N,O)(bipy)(OH_2)](NO_3)$_2$.2H_2O [44] but where the terminal bipy ligands have an anti-disposition as opposed to *syn* in **1**; the Cu atoms have square pyramidal geometries with aqua ligands in the apical positions. An anti-disposition is also found in the structure of [(phen)(bipyH)(H_2O)Cu(bipy)Cu(phen)(bipyH)(OH_2)][$Mo_{12}O_{40}P$]$_2$.2H_2O [45], i.e., with protonated terminally bound bipy ligands, where the bulky counter ions cannot approach the copper centers resulting in square pyramidal geometries again with the aqua ligands in the apical positions. Of particular interest in the structure of **1** is the mode of supramolecular aggregation occurring in the crystal.

As anticipated, conventional hydrogen bonding plays a significant role in the molecular packing of **1**, (Table S1). Thus, aqua-O–H···O(nitrate) hydrogen bonds, involving both pairs of independent aqua molecules and nitrate anions, leads to the formation of supramolecular chains along the *a*-axis. As viewed from Figure 2a, the chain is linear and as both terminal bipy molecules are oriented to the same side, the topology is of a U-tube. The remaining aqua-H atoms form hydrogen bonds to the non-coordinating pyridyl-N atoms derived from two symmetry-related U-tubes, of opposite orientation, to generate layers in the *ac*-plane and, crucially, approximately square channels parallel to *a*-axis direction (Figure 2b). The channels have disparate edge lengths and the maximum dimensions of the face, based on the Cu···Cu separations, are 8.8 x 11.0 x 12.0 x 13.1 Å. The layers stack along the *b*-axis with the primary connections between them being of the type phen-C–H···O(nitrate) (Table S1). In this way, additional channels are formed which is more symmetrical with each edge, again based on Cu···Cu separations, being 10.7 Å (Figure 2c).

Copper diimine-based honeycomb-like porous network

3.2. Catalytic activity

The catalytic ability of **1** was evaluated for the PNP's reduction into PAP using $NaBH_4$, a prototype reaction. The reduction was followed readily by UV-visible spectroscopy as both reactant (PNP) and product (PAP) absorb in the UV-visible region at different λ_{max} values [46]. Without a catalyst, the only obvious change noted was deepening of the yellow appearance of PNP upon the addition of $NaBH_4$ accompanied by a red-shift (317 nm to 400 nm), signifying the formation of PNP ions (Figure S1). The absence of a peak pertinent to PAP, even after keeping the solution for several days, indicated that the reaction required a catalyst to proceed [47]. However, in the presence of **1**, PNP to PAP conversion occurred after a few minutes as signified by the diminishing of the peak of PNP (400 nm) and the emergence of a new peak for PAP at 290 nm [48] (Figure 3a-e). In the induction period, the time required for the diffusion of reagents and catalyst, $\ln C_t/C_o$ value remains unchanged. Excess $NaBH_4$ was used, and the linearity of $\ln C_t/C_o$ vs temperature relationship indicated pseudo first-order kinetics [49]. Afterward, the catalytic conversion of PNP to PAP was studied at five different temperatures (Figure 3a-e). The induction time decreases as does the reaction time, i.e. from 22 min (25 °C) to 5 min (45 °C). Furthermore, a threefold increase in the apparent rate constant was witnessed as the temperature rose from 25 to 45 °C (Figure 4). This correlated with an increase in the average kinetic energy of molecules at elevated temperature which in turn increases the diffusion rate of the reactants. Hence, an increase in collision frequency and a fast diffusion rate triggered the conversion of reactants into products [50]. The Arrhenius equation i.e., $lnk = ln\ A - E_a/RT$, was used to calculate E_a by plotting $lnk\ vs\ 1/T$ gives a slope E_a/RT that corresponds E_a value of 40.65 $kJmol^{-1}$ [51]. The kinetic parameters such as activation entropy ($\Delta S^{\#}$) and enthalpy ($\Delta H^{\#}$) were calculated using the Erying equation i.e., $lnk/T = ln(k_b/h) + \Delta S^{\#}/R - \Delta H^{\#}/R\ (1/T)$ [52], where T is the

absolute temperature, k_b is the Boltzmann constant, h is the Planck constant, and R is the ideal gas constant. The plot of lnk_{app}/T *vs* $1/T$ gives a straight line with slope $-\Delta H^{\#}/R$ (Figure 5) and intercept ($ln(k_b/h) + \Delta S^{\#}/R$) from which $-\Delta H^{\#}$ (38.09 $kJmol^{-1}$) and $\Delta S\#$ (-197.51 $Jmol^{-1}$ K^{-1}) can be calculated (Table 2). The positive $\Delta H^{\#}$ value reflects the endothermic nature of the reduction process.

4. CONCLUSIONS

Crystallography established **1** to contain well-defined channels which, when evacuated can accommodate guest species to facilitate the conversion of environmentally detrimental PNP to pharmaceutically useful PAP. It can be envisaged that the cationic form of the complex **1**, after ionization of NO_3^-, has a high affinity for PNP and BH_4^- anions which are encapsulated in the pores to undergo the redox reaction. PNP to PAP conversion, which otherwise not possible in the absence of a suitable catalyst, completed within a few minutes in the presence of **1**. This study demonstrated that **1** with zeolite like channels can find applications as a reduction catalyst both on laboratory and industrial scales, and catalyze reactions of environmental significance.

ASSOCIATED CONTENT

Supporting Information

Supporting information contains details of the specified intermolecular interactions (Table S1) and UV-visible spectra of *p*-nitrophenol and *p*-nitrophenolate ion (Figure S1). The Supporting Information is available free of charge on the WileyPublications website.

AUTHOR INFORMATION

Corresponding Author

Copper diimine-based honeycomb-like porous network

* Zia-ur-Rehman (zrehman@qau.edu.pk / hafizqau@yahoo.com), Tel: 92-(051)90642245

Fax: 92-(051)90642241

Note

There is no conflict of interest.

ACKNOWLEDGMENT

We acknowledge the financial support from the Higher education Commission of Pakistan.

Data Availability statement

The authors confirm that the data supporting the findings of this study are available within the article and its supplementary materials.

Copper diimine-based honeycomb-like porous network

References

[1] F.-h. Lin, R.-a. Doong, *Applied Catalysis A: General* **2014**, *486*, 32-41.

[2] J. Feng, L. Su, Y. Ma, C. Ren, Q. Guo, X. Chen, *Chemical engineering journal* **2013**, *221*, 16-24.

[3] P. K. Arora, A. Srivastava, V. P. Singh, *Journal of hazardous materials* **2014**, *266*, 42-59.

[4] Z. Dong, X. Le, C. Dong, W. Zhang, X. Li, J. Ma, *Applied Catalysis B: Environmental* **2015**, *162*, 372-380.

[5] E. Marais, T. Nyokong, *Journal of hazardous materials* **2008**, *152*, 293-301.

[6] O. A. O'Connor, L. Young, *Environmental toxicology and chemistry* **1989**, *8*, 853-862.

[7] M. S. Dieckmann, K. A. Gray, *Water Research* **1996**, *30*, 1169-1183.

[8] M. A. Oturan, J. Peiroten, P. Chartrin, A. J. Acher, *Environmental Science & Technology* **2000**, *34*, 3474-3479.

[9] N. Modirshahla, M. Behnajady, S. Mohammadi-Aghdam, *Journal of hazardous materials* **2008**, *154*, 778-786.

[10] P. Canizares, C. Saez, J. Lobato, M. Rodrigo, *Industrial & engineering chemistry research* **2004**, *43*, 1944-1951.

[11] S. Saha, A. Pal, S. Kundu, S. Basu, T. Pal, *Langmuir* **2009**, *26*, 2885-2893.

[12] Y.-C. Chang, D.-H. Chen, *Journal of hazardous materials* **2009**, *165*, 664-669.

[13] a) D. Huang, G. Yang, X. Feng, X. Lai, P. Zhao, *New Journal of Chemistry* **2015**, *39*, 4685-4694; b) P. Pachfule, S. Kandambeth, D. D. Díaz, R. Banerjee, *Chemical*

Copper diimine-based honeycomb-like porous network

Communications **2014**, *50*, 3169-3172; c) R. Fenger, E. Fertitta, H. Kirmse, A. Thünemann, K. Rademann, *Physical Chemistry Chemical Physics* **2012**, *14*, 9343-9349.

[14] a) P. Zhang, C. Shao, Z. Zhang, M. Zhang, J. Mu, Z. Guo, Y. Liu, *Nanoscale* **2011**, *3*, 3357-3363; b) Z. Wang, S. Zhai, B. Zhai, Z. Xiao, F. Zhang, Q. An, *New Journal of Chemistry* **2014**, *38*, 3999-4006; c) S. Xiao, W. Xu, H. Ma, X. Fang, *RSC Advances* **2012**, *2*, 319-327.

[15] a) C. Deraedt, L. Salmon, D. Astruc, *Advanced Synthesis & Catalysis* **2014**, *356*, 2525-2538; b) Z. Wang, C. Xu, G. Gao, X. Li, *RSC Advances* **2014**, *4*, 13644-13651; c) X. Gu, W. Qi, X. Xu, Z. Sun, L. Zhang, W. Liu, X. Pan, D. Su, *Nanoscale* **2014**, *6*, 6609-6616.

[16] a) A. K. Patra, A. Dutta, A. Bhaumik, *Catalysis Communications* **2010**, *11*, 651-655; b) P. Deka, R. C. Deka, P. Bharali, *New Journal of Chemistry* **2014**, *38*, 1789-1793; c) P. Zhang, Y. Sui, G. Xiao, Y. Wang, C. Wang, B. Liu, G. Zou, B. Zou, *Journal of Materials Chemistry A* **2013**, *1*, 1632-1638.

[17] A. Goyal, S. Bansal, S. Singhal, *international journal of hydrogen energy* **2014**, *39*, 4895-4908.

[18] H. Zhang, S. Gao, N. Shang, C. Wang, Z. Wang, RSC advances, 4 (2014) 31328-31332.

[19] J. Li, L. Zhang, X. Liu, N. Shang, S. Gao, C. Feng, C. Wang, Z. Wang, New Journal of Chemistry, 42 (2018) 9684-9689.

[20] H. Zhang, Y. Zhao, W. Liu, S. Gao, N. Shang, C. Wang, Z. Wang, Catalysis Communications, 59 (2015) 161-165.

[21] B. Hoskins, R. Robson, *Journal of the American Chemical Society* **1990**, *112*, 1546-1554.

[22] P. Z. Moghadam, A. Li, S. B. Wiggin, A. Tao, A. G. Maloney, P. A. Wood, S. C. Ward, D. Fairen-Jimenez, *Chemistry of Materials* **2017**, *29*, 2618-2625.

[23] a) B. Moulton, M. J. Zaworotko, *Chemical Reviews* **2001**, *101*, 1629-1658; b) A. J. Howarth, Y. Liu, P. Li, Z. Li, T. C. Wang, J. T. Hupp, O. K. Farha, *Nature Reviews Materials* **2016**, *1*, 15018.

[24] a) K. T. Mahmudov, M. N. Kopylovich, M. F. C. G. da Silva, A. J. Pombeiro, *Coordination Chemistry Reviews* **2017**, *345*, 54-72; b) E. R. Tiekink, *Coordination Chemistry Reviews* **2017**, *345*, 209-228.

[25] a) J. Reedijk, *Chemical Society Reviews* **2013**, *42*, 1776-1783; b) N. Adarsh, P. Dastidar, *Chemical Society Reviews* **2012**, *41*, 3039-3060.

[26] a) K. Rissanen, *CrystEngComm* **2008**, *10*, 1107-1113; b) B. Li, S.-Q. Zang, L.-Y. Wang, T. C. Mak, *Coordination Chemistry Reviews* **2016**, *308*, 1-21.

[27] a) S. J. Garibay, J. R. Stork, S. M. Cohen, *Progress in Inorganic Chemistry, Volume 56* **2009**, 335-378; b) G. Kumar, R. Gupta, *Chemical Society Reviews* **2013**, *42*, 9403-9453.

[28] F. Chen, Y. Chen, H. Cao, Q. Xu, L. Yu, The Journal of Organic Chemistry, 83 (2018) 14158-14164.

[29] Y. Chen, Q. Zhang, X. Jing, J. Han, L. Yu, Materials Letters, 242 (2019) 170-173.

[30] F. Xin, Y. Rong, W. Fang, Z. Xu, X. Qing, Y. Lei, Chinese Journal of Organic Chemistry, 38 (2018) 2736-2740.

[31] D. Soriano del Amo, W. Wang, H. Jiang, C. Besanceney, A.C. Yan, M. Levy, Y. Liu, F.L. Marlow, P. Wu, Journal of the American Chemical Society, 132 (2010) 16893-16899.

[32] A.P. Ingle, N. Duran, M. Rai, Applied Microbiology and Biotechnology, 98 (2014) 1001-1009.

[33] a) A. Zanon, F. Verpoort, *Coordination Chemistry Reviews* **2017**, *353*, 201-222; b) K. Vellingiri, L. Philip, K.-H. Kim, *Coordination Chemistry Reviews* **2017**, *353*, 159-179; c) Z.

Copper diimine-based honeycomb-like porous network

Hu, D. Zhao, *CrystEngComm* **2017**, *19*, 4066-4081; d) Q. Yang, Q. Xu, H.-L. Jiang, *Chemical Society Reviews* **2017**, *46*, 4774-4808; e) L. Zhu, X.-Q. Liu, H.-L. Jiang, L.-B. Sun, *Chemical Reviews* **2017**, *117*, 8129-8176; f) C. Pagis, M. Ferbinteanu, G. Rothenberg, S. Tanase, *ACS Catalysis* **2016**, *6*, 6063-6072.

[34] S. Oh, S. Lee, M. Oh, ACS Applied Materials & Interfaces, 12 (2020) 18625-18633.

[35] M.A. Ahsan, E. Deemer, O. Fernandez-Delgado, H. Wang, M.L. Curry, A.A. El-Gendy, J.C. Noveron, Catalysis Communications, 130 (2019) 105753.

[36] M. Iqbal, S. Ali, Z.-U. Rehman, N. Muhammad, M. Sohail, V. Pandarinathan, *Journal of Coordination Chemistry* **2014**, *67*, 1731-1745.

[37] V. SAINT, *Madison, WI, USA* **2014**.

[38] S. Version, *Acta Crystallogr., Sect. A: Found. Crystallogr* **2008**, A64.

[39] G. M. Sheldrick, *Acta Crystallographica Section C: Structural Chemistry* **2015**, *71*, 3-8.

[40] O. V. Dolomanov, A. J. Blake, N. R. Champness, M. Schröder, *Journal of applied crystallography* **2003**, *36*, 1283-1284.

[41] P. SQUEEZE, *Acta Crystallographica, Section C: Structural Chemistry* **2015**, *71*, 9-18.

[42] L. J. Farrugia, *Journal of applied crystallography* **2012**, *45*, 849-854.

[43] C. Impact, *Crystal Impact GbR, Bonn, Germany* **2006**.

[44] B.-Y. Lou, M.-C. Hong, *Acta Crystallographica Section E: Structure Reports Online* **2008**, *64*, m405-m405.

[45] D.-D. Yang, B. Mu, L. Lv, R.-D. Huang, *Journal of Coordination Chemistry* **2015**, *68*, 752-765.

[46] N. Sahiner, S. Butun, O. Ozay, B. Dibek, *Journal of colloid and interface science* **2012**, *373*, 122-128.

Copper diimine-based honeycomb-like porous network

[47] M. Nasrollahzadeh, S. M. Sajadi, A. Rostami-Vartooni, M. Bagherzadeh, *Journal of colloid and interface science* **2015**, *448*, 106-113.

[48] K. Kuroda, T. Ishida, M. Haruta, *Journal of Molecular Catalysis A: Chemical* **2009**, *298*, 7-11.

[49] a) S. ur Rehman, M. Siddiq, H. Al-Lohedan, N. Sahiner, *Chemical engineering journal* **2015**, *265*, 201-209; b) X. Le, Z. Dong, W. Zhang, X. Li, J. Ma, *Journal of Molecular Catalysis A: Chemical* **2014**, *395*, 58-65.

[50] S. Wu, J. Dzubiella, J. Kaiser, M. Drechsler, X. Guo, M. Ballauff, Y. Lu, *Angewandte Chemie International Edition* **2012**, *51*, 2229-2233.

[51] M. Ajmal, Z. H. Farooqi, M. Siddiq, *Korean Journal of Chemical Engineering* **2013**, *30*, 2030-2036.

[52] a) N. Sahiner, N. Karakoyun, D. Alpaslan, N. Aktas, *International Journal of Polymeric Materials and Polymeric Biomaterials* **2013**, *62*, 590-595; b) S. Butun, N. Sahiner, *Polymer* **2011**, *52*, 4834-4840.

Figure Caption

Figure 1. Molecular structure of the binuclear copper complex, **1**.

Figure 2. Molecular packing for **1**: (a) a view of the supramolecular chain along the *a*-axis mediated by aqua-O–H···O(nitrate) hydrogen bonding, shown as orange dashed lines, (b) a view of the supramolecular layer in the *ac*-plane with aqua-O–H···N(pyridyl) hydrogen bonds shown as blue dashed lines (non-participating H atoms have been omitted), and (c) a view in projection down the *a*-axis of the unit cell contents highlighting the channels parallel to the *a*-axis.

Figure 3. Time-dependent UV-vis spectra for the reduction of PNP to PAP at five different temperatures: (a) 25, (b) 30, (c) 35, (d) 40 and (e) 45 °C.

Figure 4. ln C_t/C_o vs time graph for PNP conversion to PAP at different temperatures.

Figure 5. Plots of (a) Kapp vs temperature, (b) Ink_{app} vs 1/T (c) Ink_{app}/T vs. 1/T.

Scheme 1. Synthesis of homobimetallic copper complex, **1**.

Table 1. Selected geometric parameters (Å, °) for **1**.

Table 2. Kinetic parameters for the conversion of PNP to PAP.

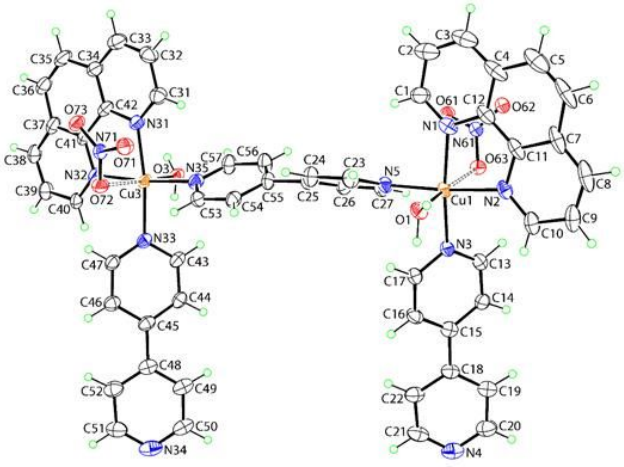

Figure 1

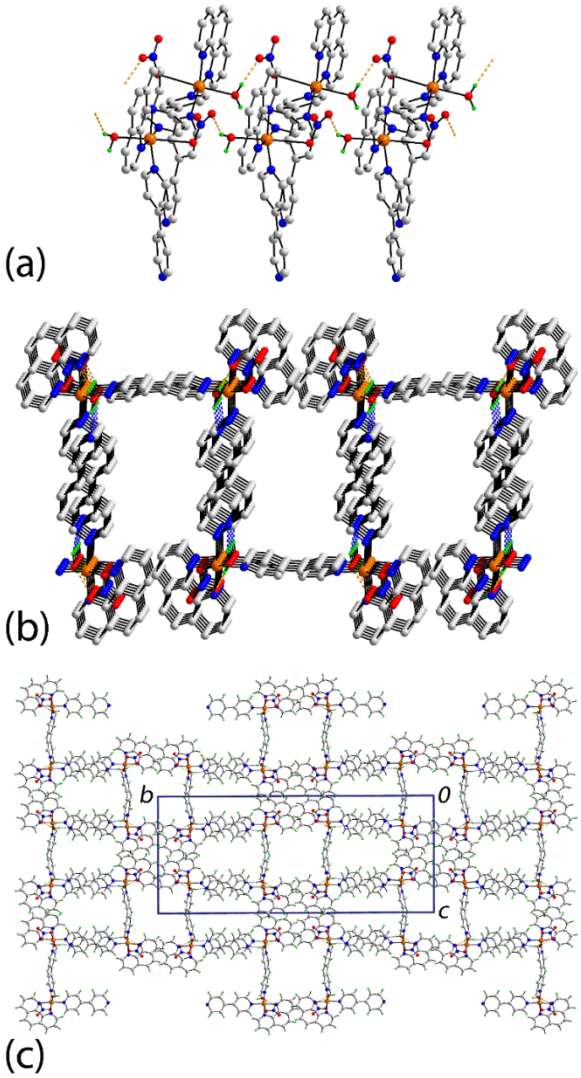

Figure 2

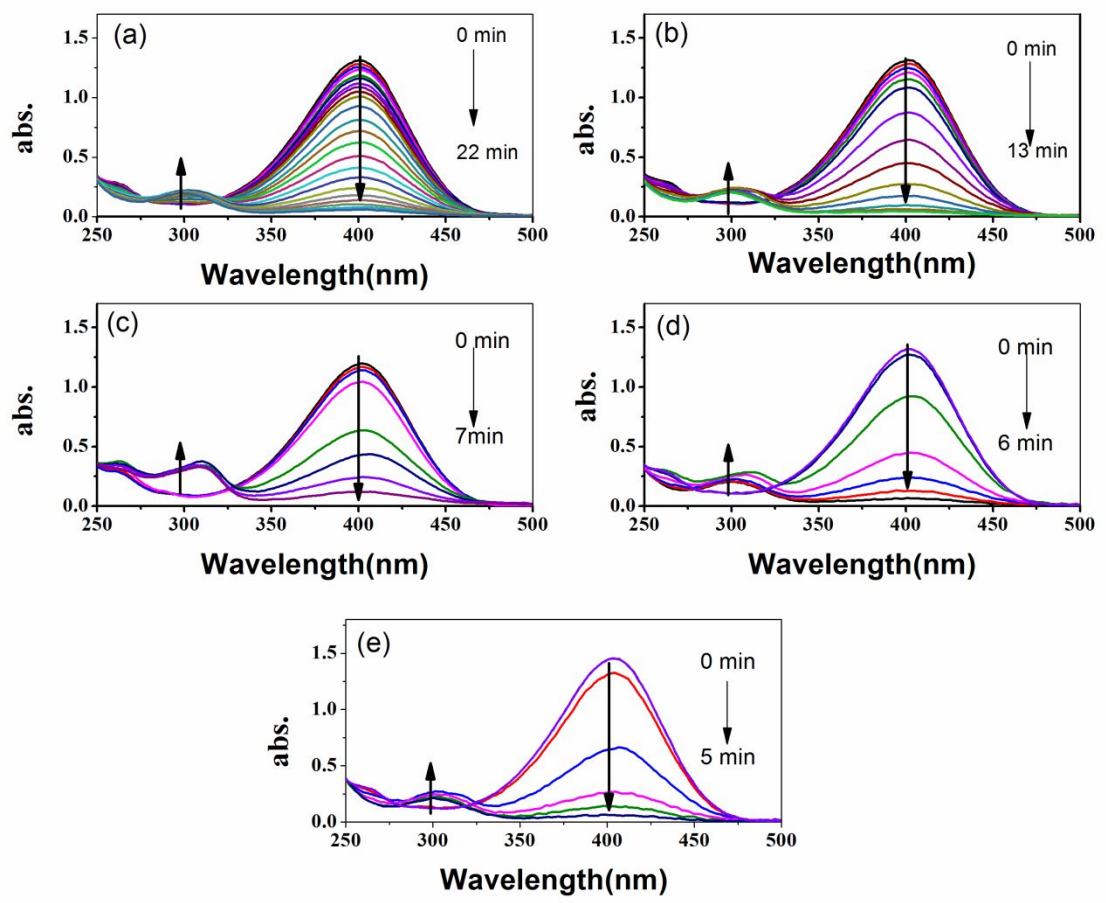
(a)
0 min
22 min
abs.
Wavelength(nm)
(b)
0 min
13 min
abs.
Wavelength(nm)
(c)
0 min
7min
abs.
Wavelength(nm)
(d)
0 min
6 min
abs.
Wavelength(nm)
(e)
0 min
5 min
abs.
Wavelength(nm)

Figure 3

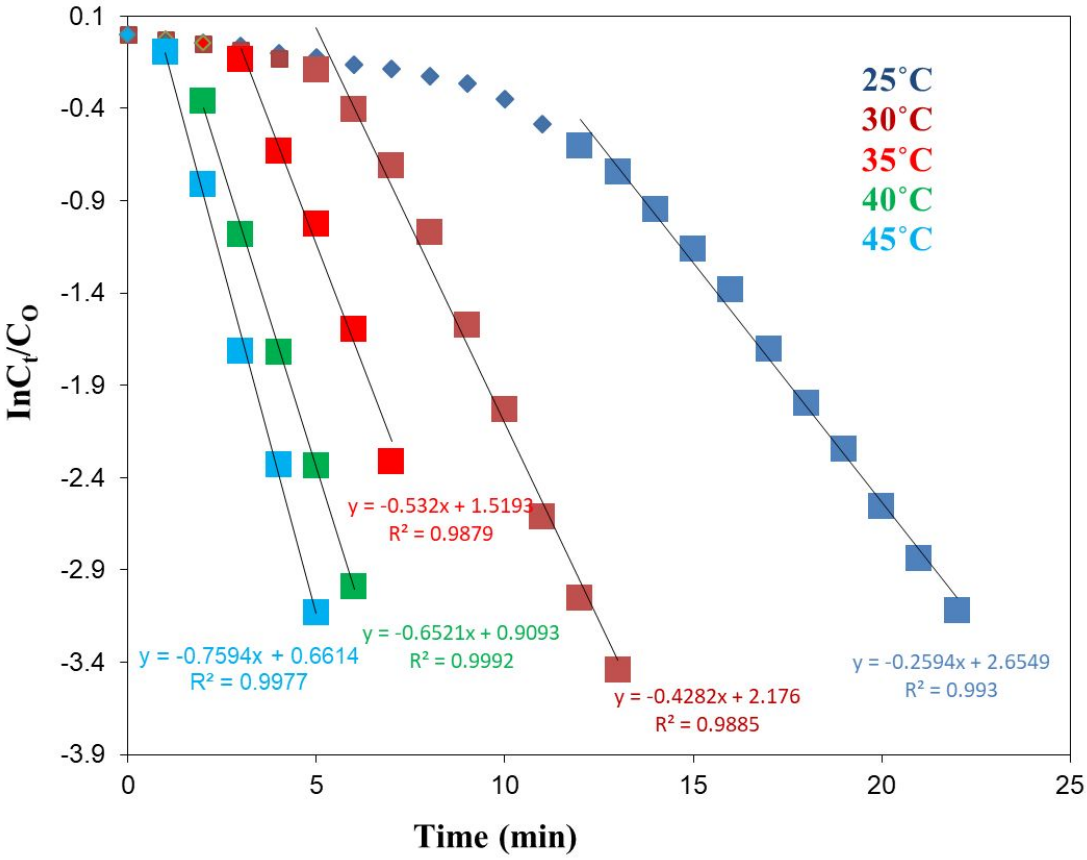

Figure 4

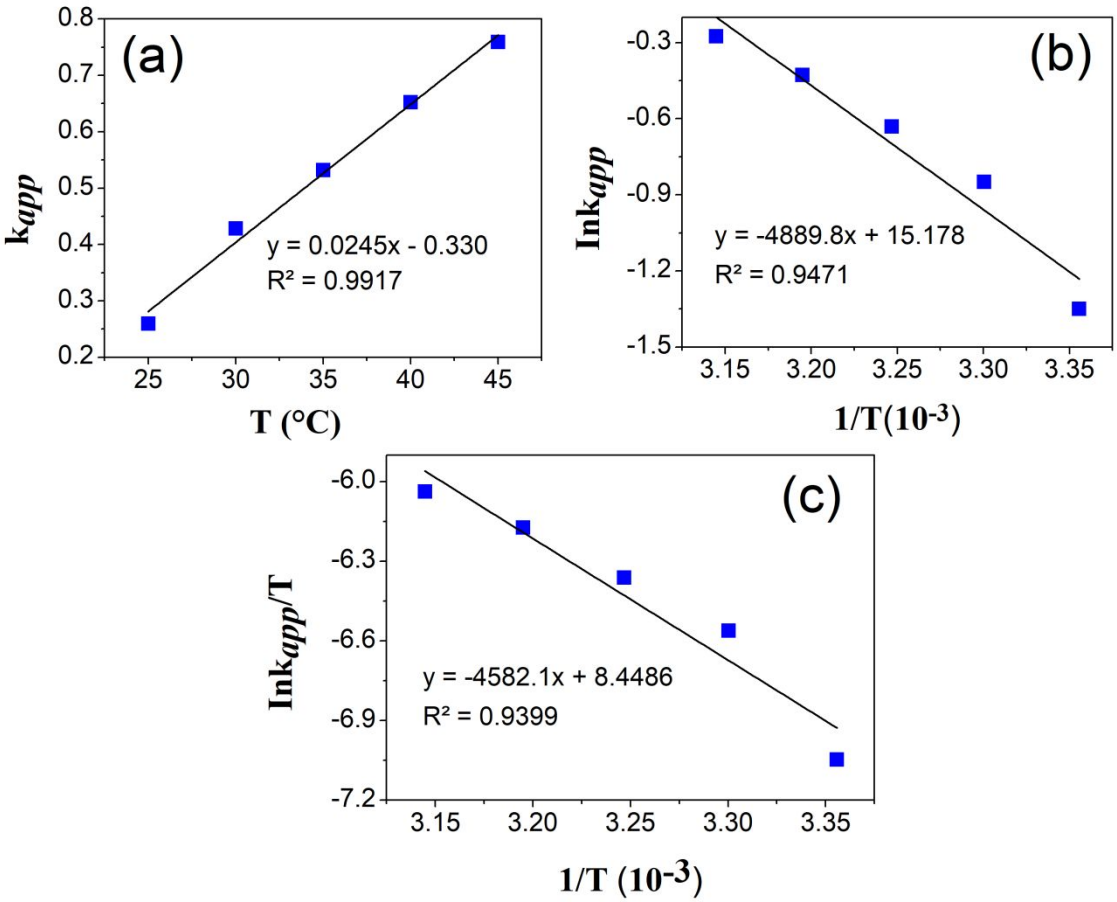

Figure 5

Table 1

Parameters	Cu1	Cu3
Cu-N(bridging bipy)	2.009(3)	1.995(3)
Cu–N(terminal bipy)	2.010(3)	2.019(3)
Cu–N(phen, trans to terminal bipy)	2.018(3)	2.015(3)
Cu–N(phen, trans to bridging bipy)	2.024(3)	2.037(3)
Cu–O(aqua)	2.265(3)	2.280(3)
Cu–O(nitrate)	2.745(3)	2.718(3)

Table 2

Temp (˚C)	K_{app} (min^{-1})	E_a (kJ/mol)	$\Delta H^{\#}$ (kJ/mol)	$\Delta S^{\#}$ (J/mol.K)	TOF (min^{-1})
25	0.259	40.65	38.09	-197.51	0.0024
30	0.428	-	-	-	0.0040
35	0.532	-	-	-	0.0075
40	0.652	-	-	-	0.0087
45	0.759	-	-	-	0.010

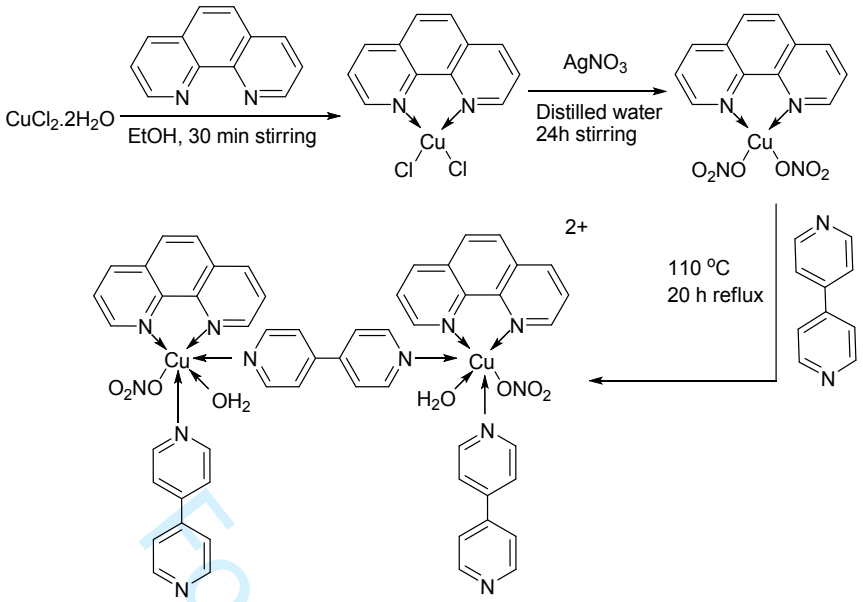

Scheme 1

Supplementary Information

A copper diimine-based honeycomb-like porous network as an efficient reduction catalyst

Abrar Ahmad[a], Syed Niaz Ali Shah[a], Mehwish Arshad[a], Francine Bélanger-Gariepy[b], Edward R.T. Tiekink[c], Zia-ur-Rehman[a*]

[a] Department of Chemistry Quaid-i-Azam University Islamabad-45320, Pakistan.

[b] Département de Chimie, Université de Montréal, Montreal, Canada.

[c] Research Centre for Crystalline Materials, School of Science and Technology, Sunway University, 47500 Bandar Sunway, Selangor Darul Ehsan, Malaysia

***Corresponding author:** Zia-ur-Rehman (zrehman@qau.edu.pk / hafizqau@yahoo.com), Tel: 92-(051)90642245 Fax: 92-(051)90642241

Table S1. Details of the specified intermolecular interactions (A–H···B; Å, °).

A	H	B	A–B	A···B	A···B	A–B···H	Symmetry
O1	H1A	N34	0.94(9)	1.95(9)	2.851(5)	162(9)	-1+*x*, 1½-*y*, -½+*z*
O1	H1B	O61	0.74(7)	2.18(7)	2.802(4)	142(8)	-1+*x*, *y*, *z*
O3	H3A	N4	0.94(7)	1.90(6)	2.826(5)	168(6)	1+*x*, 1½-*y*, ½+*z*
O3	H3B	O71	0.80(6)	1.98(6)	2.773(4)	176(5)	1+*x*, *y*, *z*
C3	H3	O73	0.95	2.56	3.435(6)	154	-*x*, 1-*y*, 1-*z*
C33	H33	O62	0.95	2.42	3.361(5)	169	1-*x*, 1-*y*, 1-*z*

Method for conversion of PNP into PAP

First of all, UV-vis spectrum of an aqueous solution of PNP (95μM) was recorded. 0.2 g of sodium borohydride was then added to a 25 mL aqueous solution of PNP (95μM) in a beaker (stock solution) from which 3 mL was pipetted out in a UV cuvette and UV-Vis spectrum was recorded again after an interval of 30 min and 24 h. To this solution, 0.12 mL of catalyst (36μM) was added followed by recording UV-vis spectra at different temperatures.

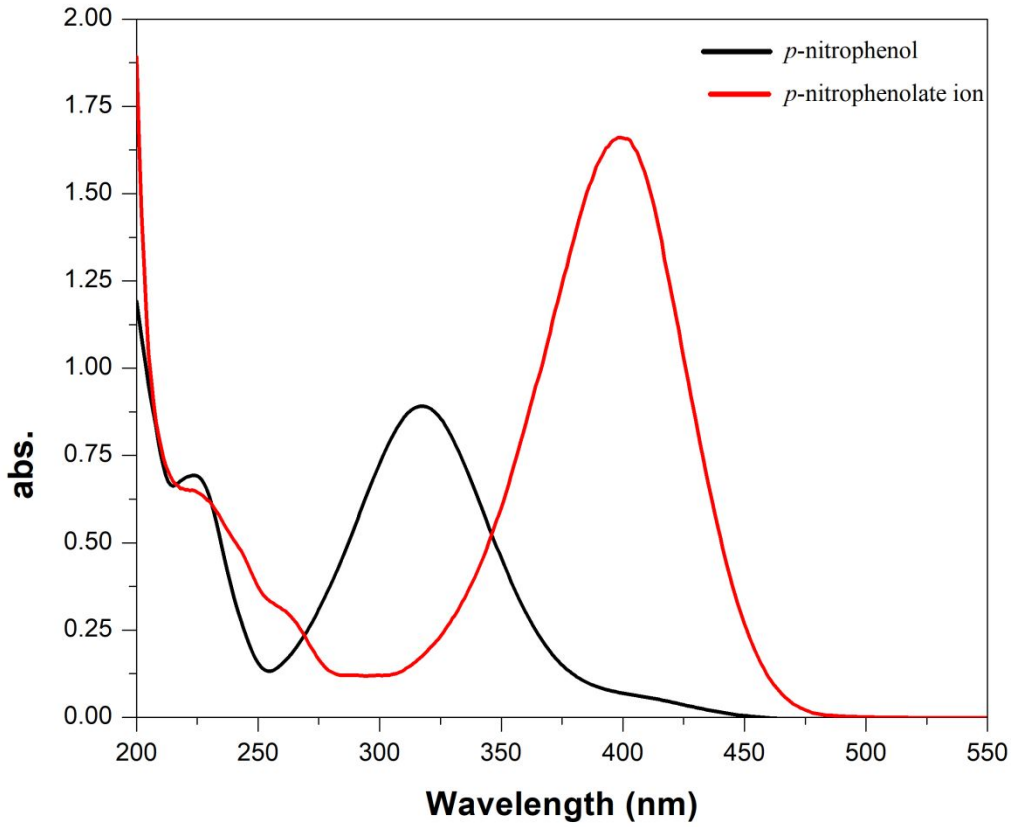

Figure S1. UV-visible spectra of *p*-nitrophenol (95 μM) and p-nitrophenolate anion in water at room temperature.

checkCIF/PLATON report

Structure factors have been supplied for datablock(s) rehma84

THIS REPORT IS FOR GUIDANCE ONLY. IF USED AS PART OF A REVIEW PROCEDURE FOR PUBLICATION, IT SHOULD NOT REPLACE THE EXPERTISE OF AN EXPERIENCED CRYSTALLOGRAPHIC REFEREE.

No syntax errors found. CIF dictionary Interpreting this report

Datablock: rehma84

Bond precision: C-C = 0.0063 A Wavelength=1.34139

Cell: a=7.3006(2) b=43.8747(10) c=18.6593(4)
alpha=90 beta=94.460(1) gamma=90
Temperature: 100 K

	Calculated	Reported
Volume	5958.7(2)	5958.7(2)
Space group	P 21/c	P 1 21/c 1
Hall group	-P 2ybc	-P 2ybc
Moiety formula	C54 H44 Cu2 N12 O8 [+ solvent]	C54 H44 Cu2 N12 O8
Sum formula	C54 H44 Cu2 N12 O8 [+ solvent]	C54 H44 Cu2 N12 O8
Mr	1116.12	1116.09
Dx,g cm-3	1.244	1.244
Z	4	4
Mu (mm-1)	4.168	4.166
F000	2296.0	2296.0
F000'	2278.64	
h,k,lmax	8,53,22	8,53,22
Nref	11319	11307
Tmin,Tmax	0.423,0.717	0.418,0.751
Tmin'	0.249	

Correction method= # Reported T Limits: Tmin=0.418 Tmax=0.751
AbsCorr = MULTI-SCAN

Data completeness= 0.999 Theta(max)= 54.916

R(reflections)= 0.0646(9908) wR2(reflections)= 0.1710(11307)

S = 1.103 Npar= 701

The following ALERTS were generated. Each ALERT has the format
test-name_ALERT_alert-type_alert-level.
Click on the hyperlinks for more details of the test.

Alert level C

```
PLAT230_ALERT_2_C Hirshfeld Test Diff for    C33    --  C34     ..        5.3 s.u.
PLAT234_ALERT_4_C Large Hirshfeld Difference C5     --  C6      ..       0.17 Ang.
PLAT341_ALERT_3_C Low Bond Precision on  C-C Bonds ..............    0.00625 Ang.
PLAT415_ALERT_2_C Short Inter D-H..H-X       H1B    ..  H27     ..       2.11 Ang.
PLAT906_ALERT_3_C Large K value in the Analysis of Variance ......      3.168 Check
PLAT911_ALERT_3_C Missing # FCF Refl Between THmin & STh/L=  0.600          6 Report
PLAT934_ALERT_3_C Number of (Iobs-Icalc)/SigmaW > 10 Outliers ....          1 Check
```

Alert level G

```
ABSMU01_ALERT_1_G  Calculation of _exptl_absorpt_correction_mu
                   not performed for this radiation type.
PLAT083_ALERT_2_G SHELXL Second Parameter in WGHT  Unusually Large      13.34 Why ?
PLAT606_ALERT_4_G VERY LARGE Solvent Accessible VOID(S) in Structure        ! Info
```

Author Response: The crystal contains highly disordered solvent (ETOH, H20) which was difficult to model. Accordingly, the MASK/OLEX2 method was used to account for the unmodelled electron density corresponding to the disordered solvent. The potential solvent volume of 1660.6 Ang^3^ corresponds to 27.9% of the unit cell volume. The calculations accounted for approximately 581.3 electrons in the unit cell. Full details are given under "_smtbx_masks_special_details"

```
PLAT794_ALERT_5_G Tentative Bond Valency for Cu1     (II)    .....       2.16 Info
PLAT794_ALERT_5_G Tentative Bond Valency for Cu3     (II)    .....       2.15 Info
PLAT868_ALERT_4_G ALERTS Due to the use of _smtbx_masks Suppressed          ! Info
PLAT910_ALERT_3_G Missing # of FCF Reflection(s) Below Theta(Min).          1 Note
PLAT912_ALERT_4_G Missing # of FCF Reflections Above STh/L=  0.600          6 Note
PLAT913_ALERT_3_G Missing # of Very Strong Reflections in FCF ....          1 Note
PLAT961_ALERT_5_G Dataset Contains no Negative Intensities .......     Please Check
PLAT978_ALERT_2_G Number C-C Bonds with Positive Residual Density.          1 Info
PLAT984_ALERT_1_G The  C-f'=     0.015 Deviates from the B&C-Value      0.014 Check
PLAT984_ALERT_1_G The Cu-f'=    -2.917 Deviates from the B&C-Value     -2.797 Check
PLAT984_ALERT_1_G The  O-f'=     0.041 Deviates from the B&C-Value      0.039 Check
PLAT985_ALERT_1_G The Cu-f"=     3.694 Deviates from the B&C-Value      3.688 Check
```

```
   0 ALERT level A = Most likely a serious problem - resolve or explain
   0 ALERT level B = A potentially serious problem, consider carefully
   7 ALERT level C = Check. Ensure it is not caused by an omission or oversight
  15 ALERT level G = General information/check it is not something unexpected

   5 ALERT type 1 CIF construction/syntax error, inconsistent or missing data
   4 ALERT type 2 Indicator that the structure model may be wrong or deficient
   6 ALERT type 3 Indicator that the structure quality may be low
   4 ALERT type 4 Improvement, methodology, query or suggestion
   3 ALERT type 5 Informative message, check
```

It is advisable to attempt to resolve as many as possible of the alerts in all categories. Often the minor alerts point to easily fixed oversights, errors and omissions in your CIF or refinement strategy, so attention to these fine details can be worthwhile. In order to resolve some of the more serious problems it may be necessary to carry out additional measurements or structure refinements. However, the purpose of your study may justify the reported deviations and the more serious of these should normally be commented upon in the discussion or experimental section of a paper or in the "special_details" fields of the CIF. checkCIF was carefully designed to identify outliers and unusual parameters, but every test has its limitations and alerts that are not important in a particular case may appear. Conversely, the absence of alerts does not guarantee there are no aspects of the results needing attention. It is up to the individual to critically assess their own results and, if necessary, seek expert advice.

Publication of your CIF in IUCr journals

A basic structural check has been run on your CIF. These basic checks will be run on all CIFs submitted for publication in IUCr journals (*Acta Crystallographica, Journal of Applied Crystallography, Journal of Synchrotron Radiation*); however, if you intend to submit to *Acta Crystallographica Section C* or *E* or *IUCrData*, you should make sure that full publication checks are run on the final version of your CIF prior to submission.

Publication of your CIF in other journals

Please refer to the *Notes for Authors* of the relevant journal for any special instructions relating to CIF submission.

PLATON version of 13/08/2017; check.def file version of 27/07/2017

Datablock rehma84 - ellipsoid plot

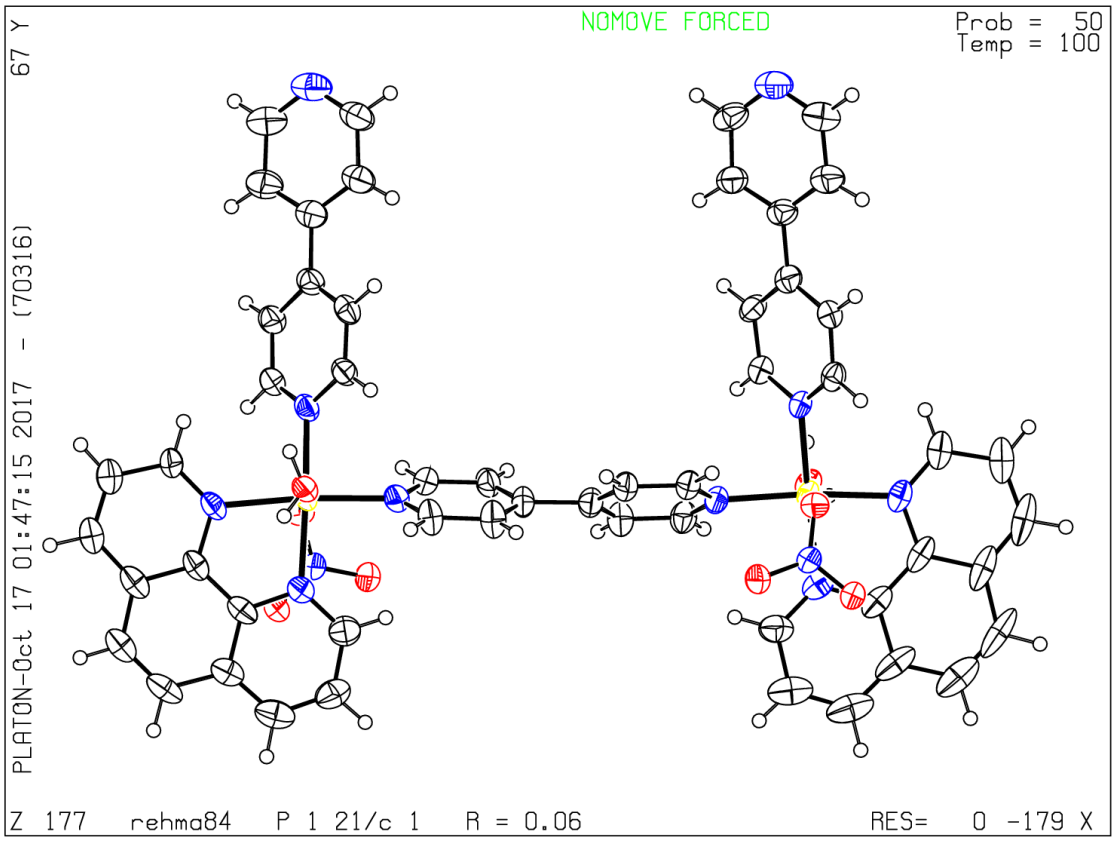

Data Availability Statement

The authors confirm that the data supporting the findings of this study are available within the article and its supplementary materials.